SSM/I Instrument Evaluation

JAMES P. HOLLINGER, JAMES L. PEIRCE, AND GENE A. POE

Abstract—**The special Sensor Microwave/Imager (SSM/I) instrument and scan geometry are briefly described. Then the results of investigations of the stability of the gain, calibration targets and spin rate, the radiometer noise and sensitivity, the coregistration, the beam width and main-beam efficiency of the antenna beams, as well as the absolute calibration and geolocation of the instrument are presented. The results of this effort demonstrate that the SSM/I is a stable, sensitive, and well-calibrated microwave radiometric system capable of providing accurate brightness temperatures for microwave images of the earth and for use by environmental product retrieval algorithms. This SSM/I, and the 11 more future ones currently built or are to be built, will provide high-performance microwave measurements for determination of global weather and critical atmospheric, oceanographic, and land parameters to operational forecasters and users and the research community for the next two decades.**

I. Introduction

THE Special Sensor Microwave/Imager (SSM/I) is flown on the Defense Meteorological Satellite Program (DMSP) Block 5D-2 F8 spacecraft in a circular sun-synchronous near-polar orbit at an altitude of approximately 833 km with an inclination of 98.8° and an orbit period of 102.0 min. The orbit produces 14.1 full orbit r/day, and has an 0613 local ascending node equatorial crossing. Fig. 1 shows the conical scan of the SSM/I in the early morning orbit. The active portion of the scan covers a swath of 1400 km, which results in the 24 h global coverage shown in Fig. 2. Only the cross-hatched areas are missed. The small circular sectors of 280 km radius at the north and south poles are never measured due to the orbit inclination, but the diamond-shaped regions will be covered after 72 h. Plans are for two SSM/I's to be in orbit at the same time, which will greatly increase the timeliness of the coverage.

The SSM/I is a seven-channel, four-frequency, linearly polarized, passive microwave radiometric system and is shown in Fig. 3. It receives both vertically and horizontally linearly polarized radiation at 19.3, 37.0, and 85.5 GHz and vertical only at 22.2 GHz. It consumes 45 W of power and weighs 48.5 kg. A high-speed momentum wheel weighing 7.3 kg is used to compensate the angular momentum of the SSM/I and is mounted separately inside the spacecraft. The SSM/I consists of an offset parabolic reflector of dimensions 61 × 66 cm, illuminated by a corrugated, broad-band, seven-port horn antenna. The reflector and feed-horn antenna are mounted on a drum which contains the radiometers, digital data subsystem, mechanical scanning subsystem, and power subsystem. The entire reflector, feed horn, and drum assembly is rotated about the axis of the drum by a coaxially mounted bearing and power transfer assembly (BAPTA). All data, commands, timing and telemetry signals, and power pass through it on slip ring connectors to the rotating assembly.

A small mirror and a hot reference absorber are mounted on the BAPTA and do not rotate with the drum assembly. They are positioned off axis such that they pass between the feed horn and the parabolic reflector, occulting the feed horn once each scan. The mirror reflects cold 3 K cosmic background radiation into the feed horn, thus serving, along with the hot reference absorber, as calibration references for the SSM/I. This scheme provides an overall end-to-end absolute calibration which includes the feed horn. A total-power radiometer configuration is employed which provides a factor of two greater sensitivity over a conventional "Dicke" switched system. Both the calibration scheme and the use of total power radiometers are innovations which significantly improve the performance of the SSM/I compared to previous spaceborne radiometric systems.

The SSM/I scan geometry is shown in Fig. 4. The SSM/I rotates continuously about an axis parallel to the local spacecraft vertical. The scan direction is from the left to the right when looking in the aft direction of the spacecraft, with the active scene measurements lying ±51.2° about the aft direction, resulting in a swath width of 1400 km. The spin rate of 31.6 r/min provides a period of 1.9 s during which the spacecraft subsatellite point, moving at 6.58 km/s, travels 12,5 km, which is nearly equal to the resolution of the 85 GHz antenna beams on the earth's surface. On each scan, 128 uniformly spaced samples of the 85.5 GHz scene data are taken over the 102.4° scan sector. The sampling interval is 4.2 ms and equals the time for the beam to travel 12.5 km in the cross-track direction. Radiometer data at the remaining frequencies are sampled every other scan, with 64 uniformly spaced samples having an 8.4 ms interval. Scan *A* in Fig. 4 denotes scans in which all channels are sampled, while Scan *B* denotes scans in which only 85.5 GHz data are taken. The start and stop times of the integrate-and-dump filters at 19.35, 22.235, and 37.0 GHz are selected to maximize the radiometer integration time and achieve concentric

Manuscript received February 14, 1990; revised April 25, 1990.

J. P. Hollinger is with the Space Sensing Branch, Naval Research Laboratory, Washington, DC 20375.

J. L. Peirce is with the Hughes Aircraft Company, Los Angeles, CA 90009.

G. A. Poe was with the Space Sensing Branch, Naval Research Laboratory, Washington, DC 20375. He is now with the Aerojet ElectroSystems Company, Azusa, CA 91702.

IEEE Log Number 9037453.

0196-2892/90/0900-0781$01.00 © 1990 IEEE

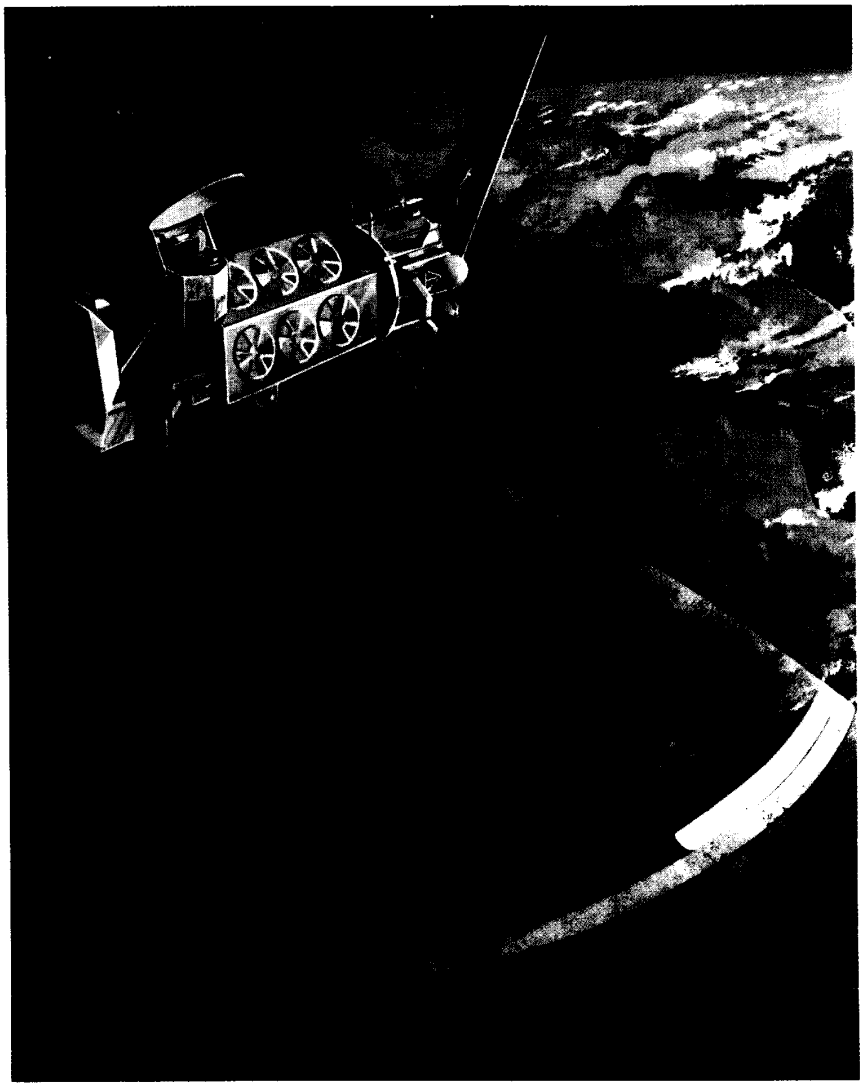

Fig. 1. Defense Meteorological Satellite Program (DMSP) Block 5D-2 satellite with the Special Sensor Microwave/Imager (SSM/I) located at the upper left.

beams for all sampled data. The effect of the radiometer integration times is to increase the effective along scan diameter and make the beams at 37 and 85 GHz nearly circular. Corrections for spillover, cross-polarization coupling, and antenna pattern effects from the parabolic reflector are incorporated in the data processing algorithms.

II. Gain Stability

The total-power receivers achieve a factor of two improvement in sensitivity over "Dicke" switched-type radiometers, but are more affected by gain variations. The SSM/I is calibrated once each scan period of 1.9 s, and the receiver gain must be constant over this interval. Gain variations over longer periods are due primarily to temperature changes, but also to aging and other effects, and are compensated for by stepping an internal gain control. Orbital variations in the sun angle, defined by the angle between the vector normal to the spacecraft's orbit and the vector from the spacecraft to the sun, and the percent of orbit not in earth shadow are shown in Fig. 5. The relatively large variation in the sun angle introduces a large variation of solar heating of the SSM/I, and consequently, large temperature changes of the instrument electronics and BAPTA. The instrument electronics have experienced temperature changes of as much as 30°C. Not only must the SSM/I survive these extreme conditions, but it must also meet radiometric performance requirements. Due to increased heating of the instrument in the winter of 1987, the SSM/I was turned off for a brief pe-

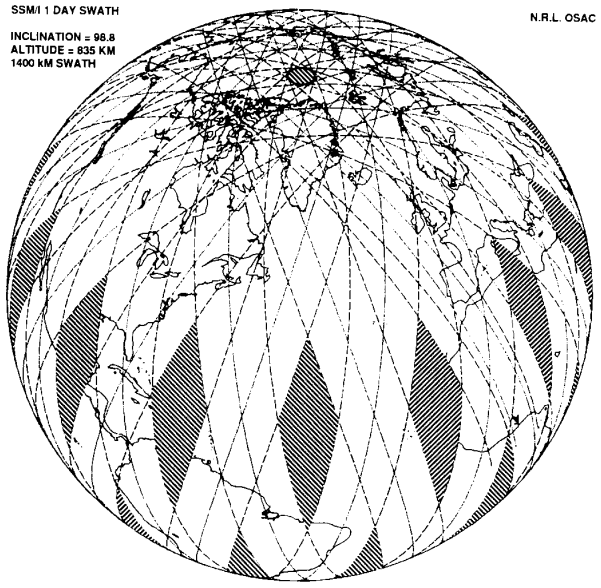

Fig. 2. Earth coverage of the SSM/I in a 24 h period. Only the shaded areas are not observed in this time period.

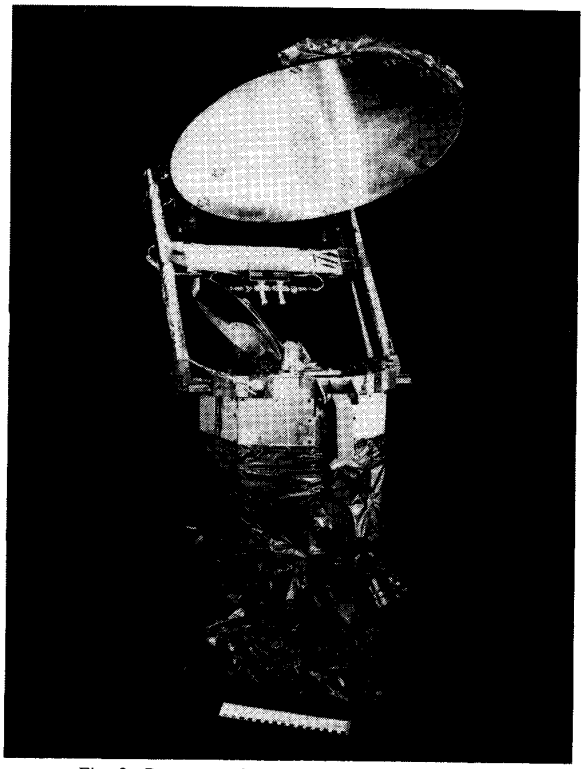

Fig. 3. Prototype of the SSM/I in deployed position.

riod from December 2, 1987 through January 12, 1988. This was done to avoid possible damage to the BAPTA when the temperature exceeded 41°C, the maximum temperature limit set by Hughes Aircraft Company. Except

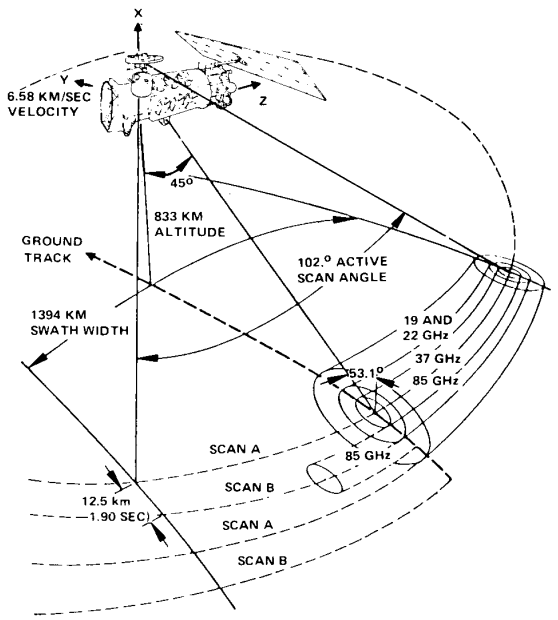

Fig. 4. SSM/I scan geometry.

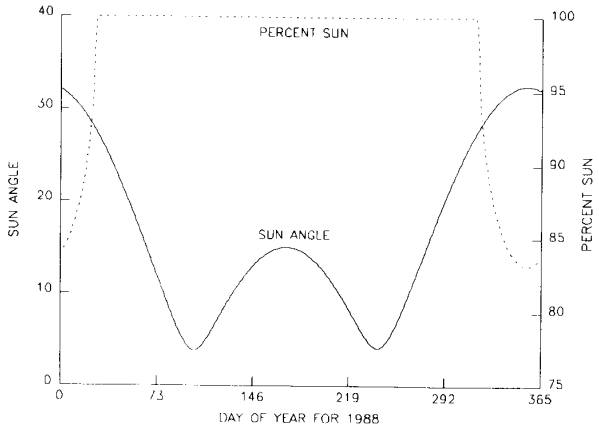

Fig. 5. Variation of the sun angle and percent sun for the DMSP F8 satellite.

for the 85 V channel, all channels returned to their performances prior to instrument turn off. The 85 V channel developed sudden gain changes and a degradation of sensitivity. Although increased heating of the instrument occurred in the winters of 1988 and 1989, the spacecraft solar arrays were repositioned to provide sufficient shading of the SSM/I to avoid the necessity of turning off the instrument. However, the 85 V channel noise continued to increase, and the channel became useless by the end of January 1989.

The automatic gain control (AGC) is designed to ensure long-term radiometer gain stability; i.e., on a seasonal basis. As the temperature of the receivers change, the power output is allowed to vary plus and minus 1 dB before a gain change is initiated. In this process, each channel samples the hot load on every scan, and commands a

gain change up when the hot load is below 7/16th of the analog-to-digital converter range (4095) or commands a gain change stepped down if the hot load for that channel is above 3/4th of the range. The stepping can occur only once every 53 s on each channel. Note that if the gain goes up and down quickly and is within the above-noted range at the end of the 53 s interval, the gain will not be stepped.

Table I presents the gain level steps for each channel since launch. The long-term gain stability is very good, except for the 85 V channel which failed. The maximum physical temperature variation experienced by the RF mixer during an orbit was approximately 2 K. This introduces less than 0.08 dB change in the radiometer gain (peak to peak) and is considerably less than the gain change needed to activate the AGC circuit. Typically, the peak-to-peak orbital gain variation observed for any of the channels was less than 0.04 dB. The effects of all scan-to-scan and long-term gain variations are accurately removed by the absolute calibration during each scan. Gain variations during a scan are not removed by the calibration, and contribute directly to the overall instrument noise. This is discussed in Section V. No RF interference either from the earth's surface or from the spacecraft has been found.

TABLE I
RADIOMETER LONG-TERM GAIN STATE SUMMARY

Channel	19 V	19 H	22 V	37 V	37 H	85 V	85 H
Date							
1987 Oct.	8	7	7	8	6	7	7
Nov.	7-8	6-7	6-7	8-9	6-7	7-8	7-8
1988 Jan.	7	6	5-6	8	6	8-9	7-8
Feb.	7	6	5-6	8	6	8	7-8
Mar.	7	6	6	8	6	8	7
May	7	6	6	8	6	9-12	7
June	7	6	6	8	6	8-11	7
July	7	6	6	8	6	8	7
Aug.	7	6	7	8	6	8-11	7
Sept.	7	6	7	8	6	8-13	7
Oct.	7	6	7	8	6	8-14	7
Nov.	7	6	5-6	8	6	9-10	7-8
Dec.	7	6	5	8	6	10-15	8
1989 Jan.	7	6	5	8	6	10	6-8
Feb.	7	6	5-6	8	6	9-10	8
Mar.	7	6	5-6	8	6	9	7
Apr.	7	6	6	8	6	9	7
May	7	6	6	8	6	9	7
June	7	6	6	8	6	9-13	7
July	7	6	6	8	6	9-13	7
Aug.	7	6	7	8	6	10-12	7
Sept.	7	6	7	8	6	10-11	7
Oct.	7-8	6-7	6-7	8-9	6	10	7-8
Nov.	7-8	6-7	6	9	6	10-11	8
Dec.	7	6	5	9	6	11	8
1990 Jan.	7	6	5	9	6	11	8

III. Calibration Target Stability

Five samples of the 85 GHz radiometer output counts are taken each 1.9 s scan when viewing the hot and cold load calibration targets. Five samples are taken every other scan at the remaining channels. The variances of these calibration load counts over the period of a revolution and for numerous revolutions were within the expected radiometric sensitivities. Further, no systematic differences were found for any of the five calibration samples taken on each scan. The result for the hot load is in agreement with the calibration results obtained during ground thermal/vacuum testing.

There were no systematic differences for any of the five calibration samples taken for the cold reflector, which is an important result since the radiometric performance of the cold reflector was not tested as a calibration reflector prior to launch. This does not mean that the samples are free from undesired contamination of spacecraft or earth emissions, which is the subject of absolute calibration of the SSM/I, but it does mean that the five samples taken on each scan agree extremely well (i.e., to within the radiometer sensitivity or noise equivalent rms radiometer output variations $NE\Delta T$). These variances were also used to estimate the SSM/I radiometer sensitivities presented in Section V.

Finally, the hot load temperatures taken by three temperature sensors at three different locations in the hot load typically varied by less than 0.5 K over a complete orbit. However, during extreme variations of solar heating at the winter solstice, variations as high as 6 K occurred. Further, the three temperatures agreed with each other, with a relative rms measurement error between the sensors of less than 0.09 K.

IV. Spin Rate Stability

The SSM/I has been spinning at a rate of once/1.8990 s, with a ± 0.0002 s variation since the initial turn-on. This translates to an azimuthal angular position error of the antenna boresight of $\pm 0.038°$. This, in turn, translates to approximately ± 0.6 km pixel position error on the earth's surface. When the SSM/I receivers were turned off for temperature control, the SSM/I continued to spin.

V. Radiometer Sensitivity

The radiometer sensitivity $NE\Delta T$ is the standard deviation of the radiometer output referenced to the energy of the radiation incident on the antenna aperture. For the SSM/I total-power radiometers, the sensitivity of each channel may be written as [6]

$$NE\Delta T = T_{SYS}\sqrt{(1/B\tau) + (\Delta G/G)^2}$$

$$T_{SYS} = T_S + T_R$$

where

T_{SYS} system noise temperature,
T_R receiver noise temperature,
T_S scene antenna temperature,
B predetection bandwidth,
τ radiometer integration time,
$\Delta G/G$ rms radiometer gain fluctuation and drift.

TABLE II
ON-ORBIT RADIOMETER SENSITIVITIES (K)
(Hot Load Target)

	Channel						
	19 V	19 H	22 V	37 V	37 H	85 V	85 H
Delta T.							
Spec. (K)	0.8	0.8	0.8	0.6	0.6	1.1	1.1
Prelaunch	0.45	0.42	0.73	0.37	0.38	0.69	0.73
On-Orbit							
June 1987	0.44	0.38	0.67	0.33	0.44	0.78	0.69
July 1987	0.38	0.34	0.59	0.32	0.32	0.75	0.62
Aug. 1987	0.37	0.37	0.58	0.30	0.33	0.69	0.59
Sept. 1987	0.38	0.35	0.63	0.29	0.33	0.73	0.60
Oct. 1987	0.45	0.42	0.69	0.35	0.44	0.87	0.70
Nov. 1987	0.46	0.42	0.74	0.40	0.52	0.91	0.78
Jan. 1988	0.50	0.44	0.74	0.42	0.58	1.12	0.85
Feb. 1988	0.43	0.41	0.72	0.37	0.42	1.32	0.75
Mar. 1988	0.43	0.41	0.69	0.33	0.35	1.48	0.73
Apr. 1988	0.42	0.39	0.70	0.33	0.37	1.70	0.70
May 1988	0.41	0.40	0.67	0.32	0.37	1.80	0.70
June 1988	0.42	0.44	0.68	0.34	0.38	1.80	0.80
July 1988	0.42	0.41	0.70	0.31	0.38	1.70	0.71
Aug. 1988	0.42	0.40	0.66	0.32	0.37	1.95	0.70
Sept. 1988	0.43	0.39	0.67	0.36	0.37	2.10	0.71
Oct. 1988	0.43	0.41	0.67	0.33	0.37	1.70	0.72
Jan. 1989	0.50	0.45	0.73	0.44	0.55	5.0	0.86
Feb. 1989	0.40	0.40	0.70	0.35	0.37	—	0.88
Mar. 1989	0.42	0.35	0.68	0.33	0.37	—	0.83
Apr. 1989	0.43	0.37	0.67	0.34	0.37	—	0.82
May 1989	0.41	0.40	0.68	0.34	0.37	—	0.89
June 1989	0.42	0.40	0.68	0.34	0.37	—	0.83
July 1989	0.42	0.40	0.68	0.34	0.37	—	0.86
Aug. 1989	0.42	0.38	0.65	0.32	0.38	—	0.89
Sept. 1989	0.42	0.40	0.65	0.32	0.38	—	0.86
Oct. 1989	0.42	0.41	0.70	0.34	0.43	—	0.90
Nov. 1989	0.42	0.42	0.73	0.36	0.51	—	0.86
Dec. 1989	0.47	0.45	0.77	0.40	0.54	—	0.85
Jan. 1990	0.46	0.43	0.75	0.38	0.51	—	0.91

Although the receiver gain fluctuation contributes directly to the $NE\Delta T$, due to the frequent radiometric calibration of the SSM/I every 1.9 s and the development of amplifiers and detectors with low $1/f$ noise, the effect of receiver gain drift is extremely small over the calibration period. Table II presents computations of the on-orbit radiometer $NE\Delta T$ for all seven channels covering the period starting when the SSM/I was turned on through January 1990. The computations are based on first computing the variance of the radiometer output counts on each scan when the SSM/I antenna is viewing the hot load calibration target, and then averaging the variances from all scans over the entire revolution. The variance in counts is referred to a variance in antenna temperature at the input of the SSM/I antenna (feed horn) using the average gain of the radiometer (K/count) computed over the revolution. Except for the channel 85 V, the sensitivities are extremely stable over the entire time period and show good agreement with the prelaunch results, except for several weeks before and after the winter solstice each year. The increase in $NE\Delta T$ in these periods is due to an increase in the temperature of the instrument and is most pronounced at 85 GHz, since these channels have the largest receiver noise temperatures. The channel sensitivities return to values noted prior to December 1987, except for the 85 GHz channels. The 85 V channel $NE\Delta T$ increased from approximately 0.8 to 2.1 K, and then in January 1989, reached 5 K just before total failure. The 85 H channel has lost some sensitivity during each warming period, and has never fully recovered its postlaunch value. Although the cause is not known conclusively, it is likely due to the mixer portion of the receiver. As noted above, the $NE\Delta T$ is strongly correlated with the instrument temperature.

Using the cold reflector calibration radiometer output counts, computations similar to those for the hot load target were made on the radiometer sensitivities. The sensitivities were found to be quite stable over the period covered by Table II, and agree with results expected when the scene brightness temperature is near 3 K: i.e., the cosmic background temperature seen by the cold reflector calibration target. The $NE\Delta T$'s are considerably lower than those of Table II, with the exception of the 85 GHz channels. For these channels, the system noise temperature is much larger than the other channels, and the scene temperature has a correspondingly smaller effect on the radiometer sensitivity. The sensitivities computed for the cold reflector target show the same trend as the data in Table II, and exhibit the same dramatic changes in sensitivity during the November–January warming periods.

VI. ANTENNA BEAM CHARACTERISTICS

Table III presents measurements of the instanteous field of view (IFOV) 3 dB beamwidths of the secondary radiation patterns as a function of channel frequency and polarization for the SSM/I. The data apply to Sensor S/N 002 on F8 and are based on antenna pattern measurements, made prior to launch, which have been averaged over the RF passbands. Similar beamwidths apply to other sensor serial numbers. Since the radiometer integrate-and-dump filter integrates the instantaneous radiometer output over 3.89 ms at 85.5 GHz and 7.95 ms at the remaining channels, an effective field of view (EFOV) may be defined for each sampled radiometer brightness temperature which takes the integration time into account. (As noted earlier, the time between samples is 4.22 ms for 85 GHz and 8.44 ms for 19/22/37 GHz channels, which includes both the integration time and time to sample and dump the data.) The EFOV is significantly larger than the IFOV in the cross-track direction (or H-plane direction) and essentially the same in the along-track direction. Table III presents the EFOV 3 dB beamwidths next to the IFOV beamwidths. Also shown are the along-track and cross-track dimensions of the EFOV beamwidths when projected onto the earth's surface.

A partial verification of these characteristics may be made by examining the response of the brightness temperatures to land/water boundaries. Such a response would resemble a step response of the antenna pattern in the cross-track direction for a coastal region lying perpendicular to the scan direction or a step response in the along-track direction for a coastal region lying parallel to the

TABLE III
SSM/I ANTENNA BEAMWIDTHS (S/N 002)

Channel Frequency (GHz)	Pol. V/H	IF Passband (MHz)	Beamwidth (Deg.)			EFOV on Earth Surface (km)	
			E Plane IFOV	*H* Plane IFOV	*H* Plane EFOV	Along-Track	Cross-Track
19.35	V	10-250	1.86	1.87	1.93	69	43
19.35	H	10-250	1.88	1.87	1.93	69	43
22.235	V	10-250	1.60	1.65	1.83	60	40
37.0	V	100-1000	1.00	1.10	1.27	37	28
37.0	H	100-1000	1.00	1.10	1.31	37	29
85.5	V	100-1500	0.41	0.43	0.60	15	13
85.5	H	100-1500	0.42	0.45	0.60	15	13

scan direction. The partial derivatives of these responses should approximate the antenna pattern in the direction of interest. These computations were done for all channels by fitting the brightness temperature responses with cubic spline functions for data taken on the western coast of the United States and the southern coasts of Africa and Australia. Fig. 6 presents the derivatives in the cross-track and along-track directions as a function of cross-track or along-track distances for the 37 GHz channel. The results exhibit the expected antenna beam characteristic in the vicinity of the maximum gain (normalized to unity), and agree quite well with the 3 dB beamwidths presented in Table III for both cross-track and along-track directions. The smaller oscillations appearing in the figure are not antenna sidelobes, but are due to variations of the scene brightness temperatures outside the coastal boundary. Similar results were obtained for the 19, 22, and 85 GHz channels. The locations of the maximum gains were within 1-2 km for all channels for a given coastal boundary, indicating that the antenna beams share a common center.

Another important antenna performance parameter is the main beam efficiency, and is defined as the percentage of energy received within the main beam of the far-field radiation pattern in the desired polarization within the prescribed bandwidth to the total energy received. The far-field antenna pattern is the combination of the radiation patterns of the feed-horn antenna and the parabolic reflector antenna. Table IV presents antenna beam efficiencies as a function of channel frequency and polarization for instrument S/N 002. The data are based on the antenna range measurements of both the feed-horn patterns and the radiation patterns from the reflector. The antenna sidelobe column denotes the percentage of the energy lying outside 2.5 times the 3 dB beamwidth of the far-field pattern when normalized to the sum of the co- and cross-polarization energies. The cross-polarization column is the percentage of cross-polarized energy appearing at the output of the feed horn and includes contributions from both the reflector and feed horn. The feed-horn spillover factor refers to the loss of the energy in the far-field pattern not intercepted by the reflector. Thus the feed-horn spillover loss is a multiplicative factor in the computation of beam efficiency.

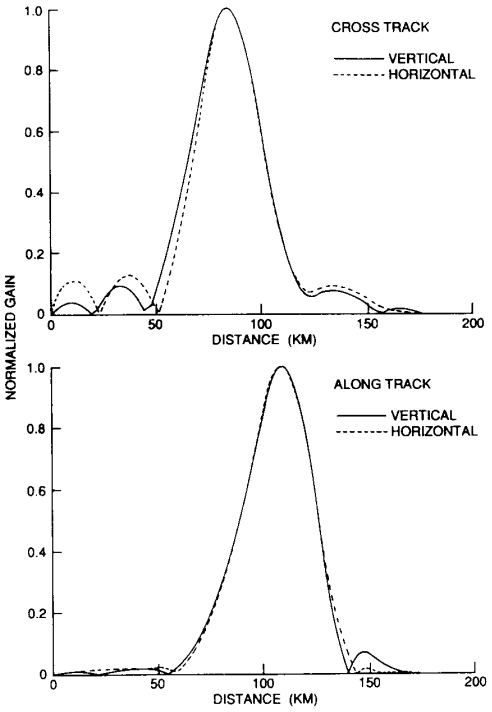

Fig. 6. 37 GHz antenna gain function derived from coastline overpasses.

TABLE IV
SSM/I BEAM EFFICIENCIES (S/N 002)

Channel Frequency (GHz)	Pol. V/H	Antenna Sidelobe (%)	Cross Polarization (%)	Feed-Horn Spillover Factor	Beam Efficiency (%)
19.35	V	0.8	0.35	0.969	96.1
19.35	H	0.4	0.30	0.969	96.5
22.235	V	2.0	0.65	0.974	95.5
37.0	V	7.3	1.80	0.986	91.4
37.0	H	4.7	1.20	0.986	94.0
85.5	V	5.7	0.60	0.988	93.2
85.5	H	7.8	1.40	0.988	91.1

Although not shown in Table IV, the loss in beam efficiency due to small-scale surface roughness of the reflector surface is very small at all frequencies. The rms

surface roughness is less than 0.025 mm, and translates to a loss of 0.8% at 85.5 GHz and less than 0.15% at the remaining frequencies. Corrections are applied to the measured antenna temperatures to remove the effects of antenna sidelobes and feed horn spillover, as well as cross-polarization coupling. The accuracy of the beam efficiency and cross-polarization corrections must be established by an overall absolute calibration of the instrument, which is discussed in Section VII.

VII. Absolute Calibration

In general, high-gain antennas like the SSM/I's receive radiation primarily over a relatively narrow "main beam" or solid angle. However, some radiation is received in antenna sidelobes in directions outside the main beam, and from reflections from the spacecraft and direct spillover into the feed horn, as well as cross-polarization coupling as discussed in Section VI. This spurious radiation must be accounted for in order to obtain the mean radiance or brightness temperature from the scene averaged over the main-beam solid angle, which is the quantity to be used in the environmental algorithms.

The evaluation of the absolute calibration of the SSM/I brightness temperatures is an extremely formidable task due to the difficulty in obtaining an accurate standard with which to compare the SSM/I. Two different methods are used. The first is a comparison of the SSM/I brightness temperatures to those derived from aircraft underflight measurements made during satellite overpass using the SSM/I simulator. The SSM/I simulator is a set of radiometers, with the same frequencies, polarizations, and incidence angle as the SSM/I, mounted in the NRL RP-3A aircraft. The second method is a comparison of the SSM/I brightness temperatures to those calculated using theoretical models.

A total of 18 SSM/I simulator underflights were made. Ten of these were over the ocean and are used for the brightness temperature calibration. The remaining flights were either in support of land and sea ice parameter validation or are not usable due to problems with the aircraft, the SSM/I simulator, or the SSM/I data. The underflights were in the form of a cross with 200 km arms. They required approximately $1\frac{1}{2}$ h, centered on the satellite overpass time, to fly. In contrast, the satellite passed over the test area in about $\frac{1}{2}$ min. The surface resolution of the aircraft SSM/I simulator radiometers is 1.5 km compared to 13–70 km, depending on frequency, for the SSM/I. The SSM/I integrates radiation over a much larger spatial region for a much shorter time than does the aircraft simulator; therefore, any significant changes in the brightness distribution over the test region during the aircraft measurements will degrade the accuracy of the simulator calibration. The ideal flight conditions are clear skies with calm seas well away from land to provide a large homogeneous region with no antenna sidelobe effects and were not always obtained.

The absolute calibration of the SSM/I simulator was established using laboratory liquid nitrogen and room temperature blackbody enclosures. This determination was tested by making rooftop zenith sky measurements in February, when the sky radiation is low and most accurately modeled, and by making measurements of a small fresh water test tank at selected incidence angles. A further test of the absolute calibration was made by flights over a fresh water lake and a heavily vegetated area near the lake under clear, calm conditions. This test site was also overflown whenever possible on the way to the ocean test site. The NRL ocean environmental model [1] was used to calculate theoretical brightness temperatures for comparison to these measurements. The absolute brightness temperature calibration of the SSM/I aircraft simulator is believed to be ± 3–4 K.

The aircraft data were corrected for small incidence angle changes due to pitch and roll of the aircraft, and for the effect of the atmosphere above the aircraft using the environmental model. All aircraft measurements are referred to an incidence angle of 53.1°. This corresponds to a measurement of the deployed boresight of the SSM/I on the DMSP satellite of 44.8° and a mean satellite altitude of 859 km. These corrections were usually less than 4 K.

The results from the SSM/I simulator flights are compared to the SSM/I brightness temperatures in Fig. 7. The differences between the SSM/I and the simulator have been averaged together for each flight to provide a single measurement pair for each SSM/I channel. The standard deviations of the means given for the SSM/I and especially for the simulator are primarily measures of the variations of the signal over the legs and are not due to instrument noise alone, which is generally less than 1 K. If the simulator signal exactly matched the SSM/I's along the track, the standard deviation of the difference between them would be dominated by instrument noise and would be less than 1 K. In this case, any bias or difference in the absolute calibration between the SSM/I and the simulator would be most accurately determined. However, the standard deviation of the difference is dominated by the effects of the mismatch in spatial and temporal scales. The average measurements from all of the flights are given in Table V.

Except for the 85 V channel, the SSM/I brightness temperatures are lower than the aircraft simulator. However, only at 37 GHz do the differences exceed 4 K. Both the SSM/I and aircraft simulator measurements have an rms scatter of 1–4 K. It is reasonable to apportion the SSM/I–simulator difference errors equally between the SSM/I and the simulator. Thus these measurements show the standard error on the determination of the SSM/I absolute calibration to be ± 3 K, and are consistent with little or no error in the SSM/I absolute brightness temperatures.

Three different regions were chosen for comparison of theoretically generated brightness temperatures to those measured by the SSM/I: 1) clear, calm ocean areas selected by having the coldest 85 GHz brightness temperatures observed over the ocean, 2) the Amazon rain forest, and 3) the Arabian desert. These regions were selected because they are homogeneous over large areas, relatively

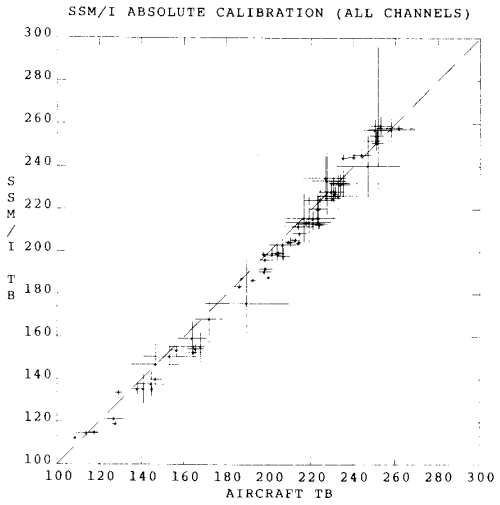

Fig. 7. SSM/I absolute brightness temperatures for all channels compared to collocated simultaneous brightness temperatures obtained from aircraft subsatellite underflights with the SSM/I simulator.

TABLE V
SSM/I SATELLITE AND AIRCRAFT BRIGHTNESS TEMPERATURE MEASUREMENTS OVER OCEAN (K)

	SSM/I	Simulator	Difference
19 V	191.6 ± 0.9	195.8 ± 1.0	−4.2 ± 1.1
19 H	122.5 ± 1.5	124.6 ± 1.6	−2.1 ± 1.7
22 V	210.7 ± 1.3	214.8 ± 1.2	−4.1 ± 1.2
37 V	211.8 ± 1.3	217.3 ± 2.0	−5.5 ± 2.2
37 H	150.7 ± 2.6	157.1 ± 3.6	−6.4 ± 3.8
85 V	250.3 ± 1.6	247.3 ± 2.6	3.0 ± 2.6
85 H	213.6 ± 4.0	215.6 ± 3.7	−2.0 ± 4.6

unchanging, and work has been done to develop models for them.

The ocean areas are the most accurately modeled of the regions selected. Under the calm sea conditions assumed to prevail for the selected SSM/I data, the ocean departs very little from a smooth dielectric interface whose radiative properties are well known. The radiative transfer of a dry cloudless atmosphere is also very well understood and widely available. The greatest uncertainty is the uniformity and degree to which the selected areas satisfy the assumption of calm, clear ocean and the uncertainty in the physical temperature of the sea. In addition, water vapor absorption is somewhat uncertain due to the need for emperical correction to the nonresonate absorption in the wings of infrared lines. This has been minimized by selecting very dry atmospheres.

The Amazon rain forest is expected to be a diffuse scatterer, unpolarized, and approximately a blackbody. The differential scattering coefficients developed by Peake [2] for a predominantly diffuse scattering surface with no specular reflection except at grazing incidence were used. These have the form:

$$\gamma(\cos\theta_0 + \cos\theta_s)/(2\cos\theta_0)$$

where atmospheric radiation incident on the surface at an angle θ_s, integrated over the upper hemisphere, is scattered into the viewing angle θ_0. The emissivity ϵ of the surface is found by subtracting the integral of the scattering coefficient over the upper hemisphere from unity and is given by

$$\epsilon = 1 - \frac{\gamma}{8}\left(\frac{1 + 2\cos\theta_0}{\cos\theta_0}\right).$$

The constant γ was taken to be 0.2, and a humid tropical model atmosphere with 5.5 cm of precipitable water vapor and a surface temperature of 29°C was used.

Modeling the Arabian desert is the least certain. There are very few data on the dielectric constant of sandy soils, and the effects of scattering and roughness especially above 19 GHz are not well known. Therefore the model brightness temperature calculations for the Arabian desert are most questionable, especially at the higher frequencies. Perhaps the best model available for the desert is to use the Fresnel reflection coefficients for a smooth dielectric interface modified by an empirical roughness factor [3]–[5]. This factor, which multiplies the Fresnel reflection coefficient, is given by $\exp -(h * \cos^2\theta)$ where θ is the incidence angle. The quantity h depends upon frequency and the scale of surface roughness, but this dependency is not known [5]. Measurements at 19.4 GHz indicate a value of 0.6 [3]. Unfortunately, no measurements above 19.4 GHz are available. The model brightness temperature calculations presented here used a value of 0.6 for h and 3 and 0.3 for the real and imaginary parts of the dielectric constant. A dry model atmosphere with 0.25 cm of precipital water vapor and a surface temperature of 29°C was used.

The SSM/I and model brightness temperature calculations are compared in Table VI. The scatter of the SSM/I is a measure of the uniformity of the samples, but the measurements may contain unknown systematic errors. As expected, the ocean and Amazon rain forest modeled brightness temperatures show the best agreement with SSM/I measurements. The Arabian desert results show poorest agreement for the 37 and 85.5 GHz channels where the effects of roughness and scattering are most uncertain in the model. With the exception of the 37 V, 85 V, and 85 H for the Arabian desert, all of the model comparisons are consistent with a standard error on the determination of the absolute calibration of the SSM/I of ±3 K. Again, there is an apparent trend for the SSM/I brightness temperatures to be lower then the modeled values, especially for the higher frequency channels. However, the uncertainty of modeling does not allow a more definite determination to be made.

In summary, all of the SSM/I simulator measurements and model calculations, with the exception of the 37 channel simulator measurements and the 37 V and 85 GHz channel Arabian desert calculations, are in good agreement with the data. The accuracy of the determination of the calibration of the SSM/I appears somewhat better at

TABLE VI
SSM/I SATELLITE AND MODELED BRIGHTNESS TEMPERATURE MEASUREMENTS (K)

	Clear Calm Ocean		
	SSM/I	Model	Difference
19 V	178.8 ± 1.0	177.7	1.1
19 H	100.6 ± 1.8	99.7	0.9
22 V	187.6 ± 2.7	187.1	0.5
37 V	202.4 ± 0.8	205.2	−2.8
37 H	129.6 ± 2.0	129.3	0.3
85 V	234.7 ± 2.2	239.0	−4.3
85 H	172.6 ± 1.6	173.7	−1.1
	Amazon Rain Forest		
	SSM/I	Model	Difference
19 V	282.1 ± 1.0	281.9	0.2
19 H	282.1 ± 1.9	281.9	0.2
22 V	282.1 ± 1.3	283.2	−1.1
37 V	278.3 ± 1.2	281.7	−3.4
37 H	277.8 ± 0.9	281.7	−3.9
85 V	283.5 ± 1.4	287.9	−4.4
85 H	283.3 ± 1.3	287.9	−4.6
	Arabian Desert		
	SSM/I	Model	Difference
19 V	299.3 ± 1.0	300.0	−0.7
19 H	256.6 ± 2.1	257.1	−0.5
22 V	296.1 ± 0.9	299.6	−3.5
37 V	292.9 ± 1.2	299.1	−6.2
37 H	257.3 ± 2.0	259.2	−1.9
85 V	287.5 ± 1.4	298.5	−11.0
85 H	268.8 ± 2.8	261.6	7.2

19 and 22 GHz, becoming less certain at 37 GHz and then 85 GHz. Although there is an apparent trend for the absolute calibration of the SSM/I to be low, especially at 37 GHz, both the aircraft simulator and model differences are consistent with little or no errors in the SSM/I absolute brightness temperatures. The present assessment of the standard error of the determination of the absolute calibration of SSM/I is that it is ±3 K. It should be noted that the excellent instrument stability and overall calibration scheme permit the effect of biases to be removed. Thus, even if a systematic error or bias is present in the absolute brightness temperature calibration, the validation and adjustment of the retrieval algorithms have removed its effect from the environmental products.

VIII. GEOLOCATION

Errors of ±25 km or more were found in the geolocation of SSM/I data. Approximately one half of this error was due to use of a seven-day predictive ephemeris in data processing. This error was removed when the satellite ephemeris was used in geolocation data processing, beginning with revolution 10 647 on July 12, 1989. There are indications that it may be possible to reduce the remaining error of about ±13 km to within specification of ±7 km by the use of a constant or slowly varying and predictable adjustment to the apparent spin axis of the SSM/I in the geolocation software. This does not necessarily mean that the SSM/I axis is misaligned with respect to the spacecraft, but only that it is possible to compensate by this means for some other error or errors in the overall system. Work is continuing on this problem. The geolocation error is considered in detail in the accompanying paper [7].

IX. CONCLUSIONS

In view of the results presented, it is clear that the on-orbit SSM/I channel radiometric sensitivities and receiver gain stabilities meet or exceed prelaunch performance specifications, except for the 85 GHz vertically polarized channel which never recovered the level of performance it had prior to when the instrument was turned off in December 1987. The instrument spin rate has been extremely stable since launch, with a maximum variation of ±0.0002 s, which translates to less than 0.6 km error in pixel location. The calibration hot load target exhibited excellent short-term stability which, in conjunction with the receiver gain stability, suggests that the calibration data taken on several adjacent scans may be averaged to improve the accuracy of the brightness temperatures. The calibration accuracy was observed to be very repeatable, providing stable brightness temperatures for a diverse set of surface types, including a number of jungle basins, deserts, and the Sargasso Sea for over a month. The absolute calibration accuracy is excellent, and may be better than the uncertainty of its determination of ±3 K. The antenna beam characteristics were examined by analyzing the step response of the SSM/I to coastal boundaries. The derived antenna patterns are consistent with beamwidths computed on the basis of antenna pattern measurements. Plots of receiver electronics, power supply, hot load calibration target, and the bearing and power transfer assembly (BAPTA) temperatures correlate well with the sun angle to the spacecraft. Although the receivers were turned off, the SSM/I experienced increased heating during the winter of 1987 and was turned off primarily to avoid damaging the BAPTA; the spacecraft solar arrays were adjusted to provide sufficient shade for the SSM/I to avoid shutting the instrument off in subsequent years. Future SSM/I's will have a modified thermal control subsystem to avoid this problem.

REFERENCES

[1] M. M. Wisler and J. P. Hollinger, "Estimation of marine environmental parameters using microwave radiometric remote sensing systems," Naval Res. Lab., Washington, DC, NRL Memo Rep. 3661, Nov. 1977.
[2] W. H. Peake, "Interaction of electromagnetic waves with some natural surfaces," *IRE Trans. Antennas Propagat.*, vol. AP-7, pp. S324–S329, Dec. 1959.
[3] B. J. Choudhury, T. J. Schmugge, A. Chang, and R. W. Newton, "Effect of roughness on the microwave emission from soils," *J. Geophys. Res.*, vol. 84, no. C9, pp. 5699–5706, Sept. 1979.
[4] W. J. Burke, T. J. Schmugge, and J. F. Paris, "Comparison of 2.8 and 21 cm microwave radiometer observations over soils with emission model calculations," *J. Geophys. Res.*, vol. 84, no. C1, pp. 287–294, Jan. 1979.
[5] T. J. Schmugge, private communication, Nov. 1988.
[6] F. T. Ulaby, R. K. Moore, and A. K. Fung, *Microwave Remote Sensing Fundamentals and Radiometry, Vol. 1.* Reading, MA: Addison-Wesley, 1981, pp. 366 -367.

[7] G. A. Poe and R. W. Conway, "A study of the geolocation errors of the special sensor microwave/imager (SSM/I)," *IEEE Trans. Geosci. Remote Sensing*, this issue, pp. 791–799.

*

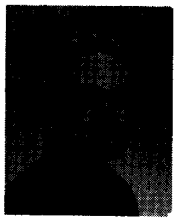

James P. Hollinger was born in Elyria, OH, on October 1, 1933. He received the B.S. degree in physics from the New Mexico Institute of Mining and Technology, Socorro, in 1956, and the M.S. degree in physics from the University of Virginia, Charlottesville, in 1958. After attending Cambridge University (England) on a Fulbright scholarship for one year, he returned to the University of Virginia and received the Ph.D. degree in physics in 1961.

After teaching physics at the George Washington University, Washington, DC, for one year, he joined the Radio Astronomy Branch at the Naval Research Laboratory (NRL), Washington, DC. Until 1969 he was principally concerned with research on the polarization and variability of radio sources and on pulsars. For the past 20 years he has worked in the area of passive microwave remote sensing. During this time he has conducted measurements from ocean towers, aircraft, and spaceborne platforms at frequencies ranging from 1.4 to 220 GHz and has published over 50 papers on microwave remote sensing. He has done extensive experiments on the microwave emission of ocean surface waves and white caps, on the quantification of marine oil spills, on the microwave properties of sea ice, and on the absorption of atmospheric molecules and hydrometeors. He participated in the specification and source evaluation boards of S-193 and S-194 flown on Skylab, on LAMMR, which was planned for NOSS, and on the SSM/I and SSM/IS flying and to be flown on DMSP. He was the Technical Manager of the LFMR instrument which was planned for N-ROSS. He led the DMSP calibration and validation of the SSM/I instrument and its geophysical retrieval algorithms and has been involved in every phase of its specification, development, and operation. He has conducted extensive airborne millimeter wave imaging measurements at 90, 140, and 220 GHz of terrain, cultural features, ships wakes, sea ice, and precipitating clouds. He has conducted studies and microwave measurements of target signatures and background clutter. He is currently Head of the Passive Microwave Section at NRL.

*

James L. Peirce received the B.S.E.E. (1962) and M.S.E.E. (1964) degrees from the University of California, Berkeley.

He has been employed by the Hughes Aircraft Company, Space and Communications Group, Los Angeles, CA, since 1965, where he has worked on the SSM/I from its inception, first as a System Engineer, and presently as Program Manager, SSM/I.

*

Gene A. Poe was born in Tulsa, OK, on March 29, 1942. He received the B.A. and M.S. degrees in electrical engineering from the University of California, Berkeley, in 1964 and 1965.

From 1986 through 1989 he worked in the Space Sensing Branch of the Naval Research Laboratory on microwave radiometric modeling and analysis of SSM/I data, as well as on radiometric target detection problems. From 1978 through 1983 he was employed by the Space and Communication Group of Hughes Aircraft Company, where he worked on microwave sensor design and retrieval algorithms of remotely sensed data. He is currently employed by Aerojet ElectroSystems Company, Azusa, CA, where he is working on advanced microwave radiometric sensor systems.